ChemPubSoc Europe

DOI: 10.1002/slct.201701699

Chemistry SELECT Full Papers

Catalysis

Electrospun Mesoporous Composite CuO−Co_3O_4/N- TiO_2 Nanofibers as Efficient Visible Light Photocatalysts

Amaresh C. Pradhan,* Anitha Senthamizhan, and Tamer Uyar*[a]

One-dimensional mesoporous composite CuO − Co_3O_4 /**N**-TiO_2 nanofibers (CuCoNT NFs) have been fabricated by *in situ* sol − gel electrospinning technique. In our approach, both polyvinylpyrrolidone (PVP) and polyethylene glycol (PEG) are used as dual polymeric carrier matrix for the fabrication of electrospun CuCoNT NFs. PVP chains assist the electrospinning of the uniform composite nanofibers whereas PEG is responsible for mesoporosity which is confirmed by N_2 sorption analyses. Along with CuCoNT NFs, other nanofiber samples (TiO_2 NFs, N-TiO_2 NFs, CuO/N-TiO_2 NFs, Co_3O_4/N-TiO_2 NFs) have also been fabricated for comparative studies. The morphology and composition of the NFs have been confirmed by the HR-TEM and XPS analyses. The red shifting of band gap energy from anatase TiO_2 NFs to composite CuCoNT NFs (1.57 eV) is suggesting formation of visible light response. Oxygen vacancies in CuCoNT NFs, leads to lowering the $e^- - h^+$ recombination. The lowering of photoluminescence spectrum and high photocurrent response in CuCoNT NFs makes CuO as low cost cocatalyst. The composite CuCoNT NFs is treated as an efficient photocatalyst for swift degradation of mixed dyes in visible light, an exemplary move. Exactly, 100% mixed dyes (30 mg/L) degradation is achieved at pH 10 in just 60 minutes.

1. Introduction

Design and construction of semiconductor photocatalysts have been extensively studied due to the strong demand for pollutants remediation to improve the environment.[1−5] Organic pollutants like dyes have detrimental effect for the whole ecosystem.[6−9] Semiconductors with various nanostructures such as nanoparticles, nanoplates, nanorods, and nanotubes have been used as a photocatalysts for degradation of organic dyes and toxic metal related pollutants and energy applications.[3,10−15]Among them, one-dimensional (1D) structures are appealing most attention due to their superior charge transport properties, few grain boundaries, and the quick ion diffusion at the semiconductor–dyes solutions interface.[16,17] Fabrication of 1D nanostructure such as nanofibers (NFs) by electrospinning is most fascinating process due to remarkable characteristics e.g., high porosity, a large surface area-to-volume ratio, and excellent substrates for secondary nanostructures.[18,19] Recently, TiO_2 NFs generated from electrospinning have been used as photocatalysis, energy, catalyst support and sensor are due to their multifunctional nature and unique properties.[20−23] Choi et al. reported that electrospinning TiO_2 NFs were more efficient than TiO_2 NPs. This is because of the interparticle photogenerated charge transport through grain boundaries, which resulting in an enhanced separation of electron-hole charge pairs.[24] Moreover, anatase TiO_2 (~3.2 eV) is believed to be the most promising and fascinating material because of its superior photoreactivity in UV region, non-toxicity, long-term stability, and low price. Hence, the design and modification of TiO_2 based NFs photocatalyst towards visible-light response are researcher's particular interest. Low cost, ease to handle and environmental friendly are the advantage aspect of visible light photocatalyst over UV light photocatalyst.

In order to tune the photoresponse of TiO_2 NFs toward visible light for efficient photocatalytic applications, following strategy may be fulfill our expectation. These are (i) construction of mesoporous and high texture TiO_2 NFs catalytic surface by sol − gel electrospinning strategy, (ii) doping of nonmetals like nitrogen (N) for visible light response, (iii) combing of CuO oxide as low cost cocatalyst and (iv) mixing of semiconductor oxide (Co_3O_4) for catalytic support. The surface texture of TiO_2 NFs can be constructed by adopting electrospinning sol − gel process. It has been noted that sol − gel electrospinning process aids to create mesoporous and well-order NFs by adding suitable optimized block copolymer template and other additive like acid and appropriate solvent.[25,26] Hence, mixing of polyvinylpyrrolidone (PVP) and polyethylene glycol (PEG) solutions are as dual polymeric carrier template for electrospinning of TiO_2 may fulfill the mesoporous NFs strategy. The vital benefit of sol − gel electrospinning process is the formation of surface hydroxyl (− OH) on the TiO_2, which is also plays a significant role in its photocatalytic activity.[27] The mesoporous nature NFs are also helps to increase the surface area which resulting high accessibility of the reacting molecules during photocatalysis. Nonmetals (nitrogen) doping into the TiO_2 has shown great potential in introducing bathochromism which encourage researchers to synthesize N doped TiO_2 based visible light active photocatalyst.[28,29] The nitrogen doping enhances the light absorption edge from the UV to the visible light region owing to the induced N 2p state.[28,30] But the

[a] *Dr. A. C. Pradhan, Dr. A. Senthamizhan, Prof. T. Uyar*
Institute of Materials Science & Nanotechnology, UNAM-National Nanotechnology Research Center, Bilkent University,
Ankara, 06800, Turkey
E-mail: uyar@unam.bilkent.edu.tr
pradhan@unam.bilkent.edu.tr

Supporting information for this article is available on the WWW under https://doi.org/10.1002/slct.201701699

oxidation/reduction potential of photogenerated charge carriers decreases are due to the interband state, which affect the efficiency of photocatalysis.[31] In order to overcome this problem, a suitable metal oxide cocatalyst is necessary to excel the photocatalytic activity. Wang et al. reported that nanostructured $Cu_2O/BiVO_4$ shows high photocatalytic degradation of methylene blue under visible light irradiation.[32] The advantages of mixing of CuO and Co_3O_4 semiconductors into the N-TiO_2 are as follow; (a) after inter-mixing of both semiconductors into the N-TiO_2, the band gap energy will be narrow and will be suitable for visible light response, (b) the mixing of three components CuO, Co_3O_4 and N-TiO_2 will enhance the physico-chemical properties, (c) the introduction of fewer amounts of CuO as compared to Co_3O_4 into N-TiO_2, is to treat CuO as cocatalyst and Co_3O_4 as supporting semiconductor. CuO (1.5 eV) is an important p-type metal oxide which is able to work under visible light.[33] The photogenerate electron acceptor and suppress the recombination of photoexcited electron–hole pairs are the two vital functions of CuO in the composite material, which will make CuO as an efficient cocatalyst in order to improve and promote photocatalytic activity in visible light.[34] Hence, *in situ* modification of CuO into the N-TiO_2 nanofibers (NT NFs) may fulfill our efficient photocatalyst strategy and suppress the electron – hole recombination. The photogenerated holes and electrons can be suppressed by fabricating a heterojunction semiconducting materials, which helps to increase the photocatalytic process. Basically, when a p-type semiconductor like Co_3O_4 combined with n-type TiO_2, the induced electric field at the heterojunction may drive the spatial separation of electron – hole, and thus increase the photocatalytic activity. Hence, *in situ* modification of Co_3O_4 into the CuO/N-TiO_2 NFs composite may suppress the photogenerated electro – hole significantly and leads to a proficient photocatalytic degradation of mixed dyes of methylene blue (MB) and methyl orange (MO).

Herein, we report the practical approach for the fabrication of mesoporous composite CuO – Co_3O_4/N-TiO_2 nanofibers (CuCoNT NFs) by *in situ* sol – gel electrospinning process. The dual polymeric templates (PVP and PEG) have taken the key role for the fabrication of above said electrospun mesoporous composite NFs. The high molecular weight PVP helps the electrospinning of the uniform nanofibrous structure whereas the low molecular weight PEG matrix is responsible for formation of mesoporous structure within composite CuCoNT NFs, which is very vital approach for the present study. *In situ* modification and construction of semiconductor oxides TiO_2, CuO and Co_3O_4 within composite NFs, enhances the morphology, textural property and photocatalytic activity in visible light which are the important advantages of the present study.

2. Results and Discussion

2.1 Mesoporosity of the NFs

N_2 sorption isotherms and the pore diameter distributions of all the NFs are shown in Figure 1, and summary of the specific surface area, pore volume and pore diameter data is shown in

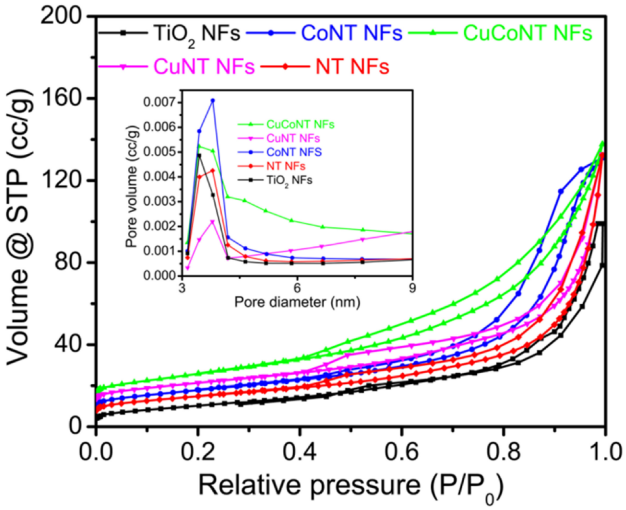

Figure 1. N_2 sorption isotherm and pore diameter of the TiO_2 NFs, NT NFs, CuNT NFs, CoNT NFs and CuCoNT NFs using mixed template PVP and PEG. The mesoporous NFs are formed at the calcination temperature at 450 °C e for 4 h.

supporting information (Table S1). All the NFs are of typical type IV isotherms with H1 hysteresis loop according to the Brunauer–Deming–Deming–Teller (BDDT) classification, suggesting the presence of mesoporous structure.[35] It is observed for all NFs that the hysteresis loop starts below 0.5 relative pressure (P/P_0) region, which is indicating intraparticle mesoporosity.[36] The formation of mesoporous structure within NFs is due to the removal of mixed PVP and PEG polymer matrix at calcinations temperature at 450 °C for 4 h. The pore size distribution curve of all NFs is shown in the Figure 1 (inset). The intense peak of all NFs is belongs to the 3–4 nm, resulting mesoporous structure.[35] The high specific surface area, pore diameter and pore volume of the NFs are listed in Table S1. The surface area of TiO_2 NFs, NT NFs, CoNT NFs, CuNT NFs and composite CuCoNT NFs are 44, 46, 52, 54 and 73 m^2/g, respectively. The high surface area of NFs will provide the more rective sites for an interaction with mixed dyes molecules. The pore diameters (Table S1) are in the range of the mesoporous scale. Hence, from the BET isotherm and pore diameter data, it is concluded that all NFs have mesoporous character within framework.

2.2 Morphological analyses of NFs

The morphologies of the nanofibers are investigated by SEM imaging. Figure 2 depicts the morphology of different nanofibers (NFs) before and after calcination. As PVP and PEG were used as carrier polymeric matrix for the electrospinning of nanofibers, the nanofibrous materials before calcination (dried 70° C for 6 h) are denoted as e.g. PVP/TiO_2 – PEG and after calcination (removal of PVP and PEG at 450 °C, 4 h), TiO_2 NFs are formed. The other NFs can be symbolized in the similar way for describing the SEM morphology. The average diameter of NFs is measured for all samples. A well-order, bead-free, and

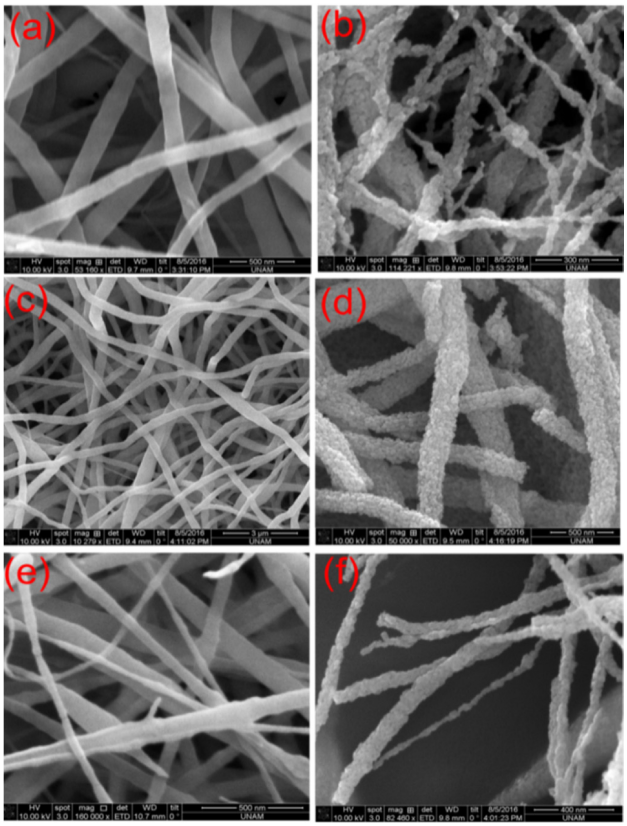

Figure 2. Representative SEM images of (a) PVP/TiO_2 – PEG, (b) TiO_2 NFs, (c) PVP/NT – PEG, (d) NT NFs, (e) PVP/CuCoNT – PEG and (f) CuCoNT NFs.

smooth diameter (80 ± 65 nm) of PVP/TiO_2 – PEG NFs is obtained before calcination (Figure 2a). The removal of PVP and PEG is occurred when PVP/TiO_2 – PEG is calcined at 450° C for 4 h, which resulting well-order, rough/mesoporous and narrow diameter (55 ± 35 nm) TiO_2 NFs (Figure 2b). Similarly, bead-free and smooth fibrous morphology are also observed for the samples PVP/N-TiO_2–PEG (PVP/NT – PEG) and PVP/CuCo–N-TiO_2–PEG (PVP/CuCoNT – PEG) NFs having diameter 300 ± 250 nm and 110 ± 80 nm in Figure 2c and 2e, respectively. Surprisingly, the reduction of diameter, creation of rough and sponge morphology enriched with mesoporous NT NFs having diameter 85 ± 70 nm are obtained (Figure 2d). Likewise composite CuCoNT NFs show rough and sponge morphology NFs having diameter 80 ± 50 nm (Figure 2f). Moreover, smooth and bead-free morphology of PVP/CuNT – PEG having diameter 160 ± 85 nm in supporting information (Figure S1a) are changed to sponge like rough/mesoporous NFs having diameter 55 ± 35 nm of composite CuNT NFs are obtained in Figure S1b. Similarly, the changed in NFs diameter, bead-free and smooth fibrous morphology of PVP/CoNT – PEG (95 ± 85 nm) to composite CoNT NFs (75 ± 55 nm) having rough and sponge mesoporous NFs morphology are obtained in the Figure S1c and S1d, respectively.

In order to check the role of PEG as a polymer matrix for the formation of the mesoporosity, for a proof-of-concept study, only PEG template is used for CuNT system. Since PEG is a low molecular weight matrix, electrospraying occured in stead of electrospinning which resulted in CuNT-PEG nanoparticles (NPs) in stead of nanofibers. The inter-connected NPs with inner gap are indicating the porosity nature of CuNT NPs. Then, the CuNT NPs are obtained by removal of PEG matrix at 450 °C in 4 h (Fig S2a). The N_2 sorption isotherm and pore diameter of the CuNT NPs is given in Figure S2b. The isotherm curve (type IV) and pore diameter (3.66 nm,Table S1) are indicating the mesoporous nature of CuNT NPs, which is prepared by PEG route. Hence, it is concluded that PEG has vital role for the formation of mesoporosity within all NFs. The decrease of fibers diameter for all NFs after calcination is due to the removal/decomposition of PVP matrix, whereas roughness/mesoporous morphology is created by the quick decomposition of low molecular weight PEG matrix. In other words, removal of high molecular weight (PVP) and low molecular weight (PEG) polymeric templates are responsible for the narrowing of NFs diameter and creating rough/mesoporous nature of NFs, respectively.

In order to investigate the morphological features of NFs, TEM and HR-TEM analyses have been performed (Figure 3). The

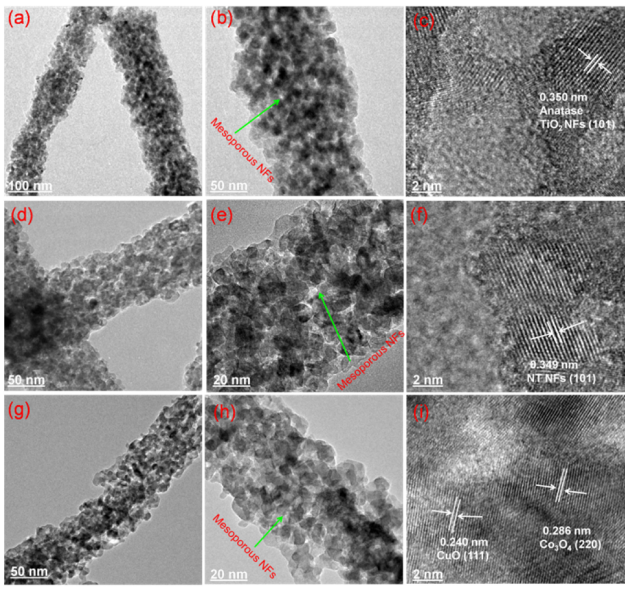

Figure 3. The representative micrographs of TiO_2 NFs (a) TEM image, (b) HR-TEM image and (c) lattice fringes; micrographs of NT NFs (d) TEM image, (e) HR-TEM image and (f) lattice fringes; micrographs of composite CuCoNT NFs (g) TEM image, (h) HR-TEM image and (i) lattice fringes.

TiO_2 NFs having mesoporous morphology are displayed from TEM and HR-TEM images in the Figure 3a and b, respectively. The lattice spacing of 0.350 nm is due to the anatase TiO_2 NFs for the plane (101), is shown in Figure 3c. The TEM, HR-TEM and lattice spacing of N-TiO_2 nanofibers (NT NFs) are shown in the Figure 3d – f. This result indicates that the mesoporous nanofibers (NFs) nature of N doped anatase TiO_2 having lattice spacing 0.349 nm for (101) plane. The slight decrease of lattice spacing in NT NFs as compared to TiO_2 NFs is may be due to

the doping effect of N into the TiO_2. Figure 3g – i shows the TEM, HR-TEM, and lattice spacing of composite CuCoNT NFs, respectively.This result indicates the mesoporous nature of CuCoNT NFs. The lattice spacing of 0.349, 0.240 and 0. 286 nm are due to the presence of N-TiO_2 (NT), CuO and Co_3O_4 ,respectively, within the composite CuCoNT NFs.[37,38] The mesoporous NFs structure of composite CuNT NFs are confirmed by TEM and HR-TEM images (Figure S3a,b). The presence of CuO and N-TiO_2 in composite CuNT NFs has been confirmed by lattice fringes (Figure S3c). Figure S3d,e also shows the mesoporous nature of composite CoNT NFs, confirmed by TEM and HR-TEM images. The lattice spacing of 0.349 and 0.286 nm correspond to the N-TiO_2 and Co_3O_4 in composite CuNT NFs (Figure S3f).

The selected area electron diffraction (SAED) patterns of all mesoporous NFs are shown in the Figure S4a–e. The prominent SAED patterns of TiO_2 NFs and NT NFs are indicating crystalline nature. The plane (103) is due to the N-doped TiO_2 (NT). The very clear ring patterns of CuNT NFs, CoNT NFs and CuCoNT NFs are indicating the polycrystalline nature. The planes (110) and (111) are characteristics of CuO in CuNT NFs whereas planes (220) and (311) are due to the Co_3O_4 in CoNT NFs. Finally, the combination of planes (110), (111), (220) and (311) are due to the presence of CuO and Co_3O_4 in composite CuCoNT NFs.Thus, it is anticipated that the crystalline and polycrystalline nature of all mesoporous NFs would increase the light absorption efficiently. The STEM-EDAX mapping (Figure S5) results revealed the high content of Ti as compared to Cu and Cu in CuCoNT NFs, which is consistent with the experimental condition. The elemental mapping also describes the existence of N as dopant and reactive sites Cu, Co and Ti. The most important observation is that mesoporosity are also detected in the mapping of respective elements. The STEM – EDX spectroscopy is used to characterize the composition of the TiO_2 NFs, NT NFs and CuCoNT NFs, which are shown in the Figure S6. The peak intensities of elements indicates the corresponding NFs materials. Conclusively, from SEM study, the smooth NFs (before calcination) are due to the formation of metal oxide composite with PVP and PEG. The diameter reduction, formation of rough/mesoporous NFs and crystal phase of oxides within composite (after calcination) are due to the decomposition of PVP and PEG, confirmed by SEM, HR-TEM and lattice fringes.

2.3 Optical analyses of NFs

The UV-visible absorption spectra of all the NFs are shown in the Figure 4. All the NFs showed strong absorption band at 200 – 300 nm, is due to the ligand to metal charge transfer (LMCT) between oxygen and metal center within the NFs.[39] Except TiO_2 NFs, a remarkable increase in the absorption (~ 400 nm) in composite NFs, is due to the interfacial charge transfer in between TiO_2 to the metal ions.[40] Moreover, a strong absorption in the visible range is due to the red shifts in the band gap transition of the samples. This ascribes the strong electronic interaction of all semiconductor oxides includes TiO_2, CuO and Co_3O_4 within composite NFs to the influence of

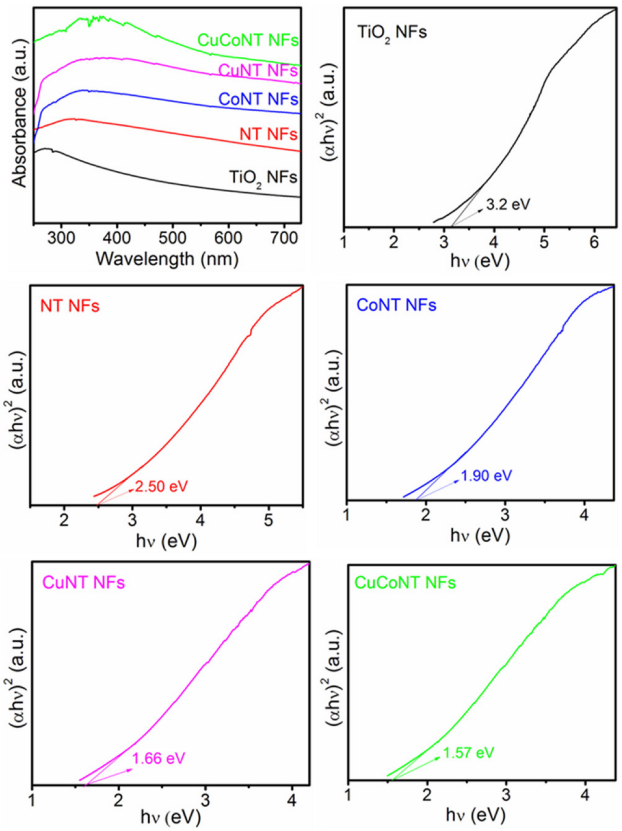

Figure 4. UV-Visible spectra and plots of $(\alpha h\nu)^2$ vs. photon energy ($h\nu$) for the band gap energy of different NFs.

charge delocalization. Thus except TiO_2 NFs, the NT NFs and other composite NFs have more affinity towards visible light. The red shifting is shifted from NT NFs to composite CuCoNT NFs which may be due to the formation of oxygen vacancies.[41] The formation of oxygen vacancies is due to the creation of Ti^{3+} after mixing of N, Cu and Co. This oxygen vacancies are creating an impurity band below the conduction band of TiO_2. This has caused the red shifting of band edge.[42] Further, the red shifting is because of the NFs morphology, which favors an efficient light absorption ability. The red shifting of all composite NFs is favoring high photocatalytic application in visible light. Hence, composite CuCoNT NFs has high red shift which is due to the involvement of more oxides semiconductor.This phenomenon enables high photocatalytic applications in visible light. The band gap energy of all mesoporous NFs materials can be calculated by using the equation 1.[43]

$$\alpha h\nu = A(h\nu - Eg)^n \quad (1)$$

where α, ν, A, E_g and h are the absorption coefficient, light frequency, proportionality constant, band gap and Planck's constant, respectively. The band transition depends upon the value of n =1/2 for direct and 2 for indirect transition, respectively. It is found that all the NFs show direct allowed transitions. The band gap energies of the all mesoporous NFs

can be estimated from the plots of $(\alpha h\nu)^2$ versus photon energy ($h\nu$). The intercept of the tangent to the X axis would give a good approximation of the band gap energies for the synthesized products, as shown in Figure 4. Figure 4 also shows the band gap of TiO_2 NFs is 3.2 eV, which confirms the anatase phase. The band gap energy of NT NFs is 2.50 eV, the band gap narrowing (BGN) as compared to TiO_2 NFs is due to the formation of a localized state by mixing of N 2p and Ti 2p. Likewise, the band gap energy of CoNT NFs is 1.90 eV. This is because the formation of localized state by mixing of Co 2p, N 2p and Ti 2p. Clearly, formation of Co 2p and N 2p localized states above the valence band of TiO_2 NFs, leads to BGN as compared to TiO_2 NFs.

The band gap energy of CuNT NFs is 1.66 eV, which is due to the formation of localized states by intermixing of Cu 2p, N 2p and Ti 2p. Moreover, the band gap energy of CuCoNT NFs is 1.57 eV. The high BGN as compared to TiO_2 NFs is due to the formation of localized states by mixing of Cu 2p, Co 2p, N 2p and Ti 2p. Hence, the red shifts are observed from semiconductor NT NFs to composite CuCoNT NFs, which are due to the progressive formation of localized states. Conclusively, except TiO_2 NFs, the aforesaid semiconductor composites NFs will harvest energy from visible light for an efficient photocatalytic degradation of organic pollutants such as dyes.

2.4 Crystallinity analyses of NFs

The XRD pattern of TiO_2 NFs, NT NFs, composite CoNT NFs, CuNT NFs and CuCoNT NFs are shown in the Figure 5. The XRD

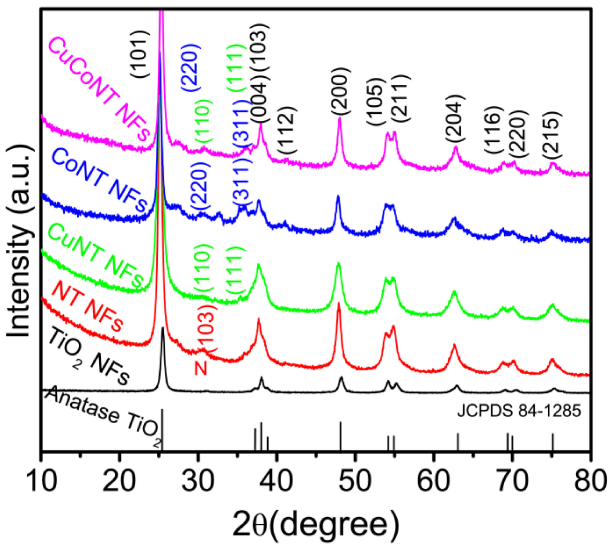

Figure 5. The X-ray diffractograms of TiO_2 NFs, NT NFs, CuNT NFs, CoNT NFs and CuCoNT NFs.a

pattern of TiO_2 NFs, the Bragg reflections at angles of 25.3°, 38°, 48°, 54°, 55°, 63°, 69°, 70° and 75° correspond to (101), (004), (200), (105), (211), (204), (116), (220) and (211) for crystal plane of anatase phase TiO_2.[44] All the peaks are perfectly indexed to JCPDS no. 84–1285. A small peak at angle $(2\theta) = 30.8^\circ$ for (103) plane, corresponds to the nitrogen mixed in TiO_2 (NT NFs).[45] Expect pure TiO_2 NFs, this nitrogen peak is available for all semiconductor oxide modified with nitrogen TiO_2 nanofibers. A signature peak at $(2\theta) = 31^\circ$ and 35°, corresponding to the plane (110) and (111), respectively, along with N mixed TiO_2 peaks, are due to the presence of CuO in N mixed TiO_2 nanofibers (CuNT NFs).[38,46]

The other peaks of CuO are dominated due presence of high amount of TiO_2. The formation and composition of Co_3O_4 in N mixed TiO_2 are identified by the two signature plane (220) and (311) are at 31° and 36°, respectively.[47] The *in situ* formation of dual semiconductor oxides CuO and Co_3O_4 in N mixed TiO_2 is due to the presence of signature planes of (110) and (111) for CuO, and (311) and (220) for Co_3O_4. Hence, the sustainability of anatase TiO_2 in all samples indicates the high light absorption for photocatalytic application.

2.5 Chemical structure analyses of NFs

XPS analysis has been performed to investigate the electronic environment and oxidation state of composite CuCoNT NFs (Figure 6).The Figure 6a, the peak at ca. 399.6 eV is generally

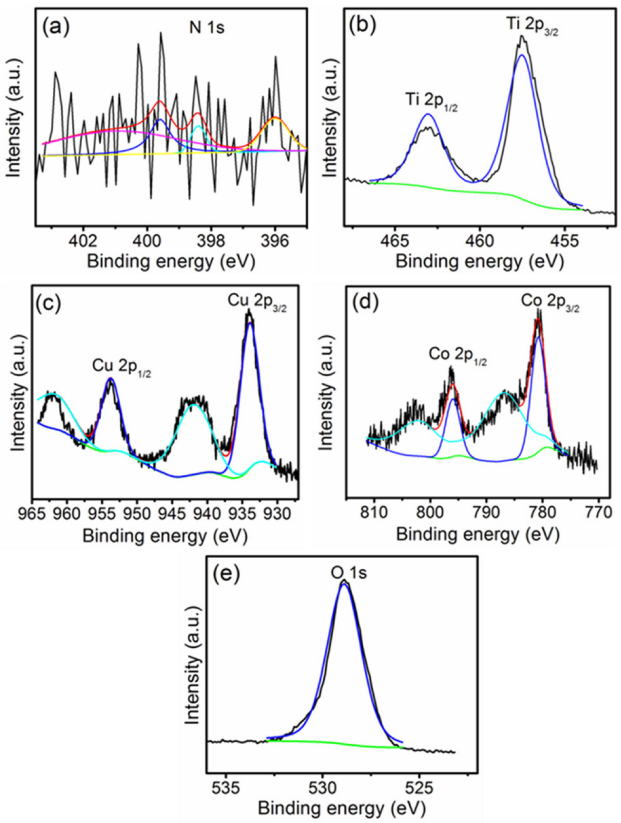

Figure 6. Core level XPS of composite CuCoNT NFs (a) N 2p spectrum, (b) representative Ti 2p spectrum, (c) Cu 2p core level spectrum, (d) Co 2p spectrum and (e) O 1s spectrum.

known asanionic N in O–Ti–N linkages.[48,49] The BE at ca. 398.4 eV refers to N^- species substituted for O^{2-} in the TiO_2 lattice.[50–52] This substitutional N doping is most effective and mainly responsible for the visible light absorption, which leads to form a localized N 2p state just above the valence band of TiO_2. This phenomenon aids to increase the photocatalytic activity in the visible region. The weak N1s peak at ca. 401 eV is attributed to the presence of oxidized nitrogen, e.g., Ti–O–N, Ti–N–O linkages.[53] This leads to the strong interaction between N and O, which is beneficial for interstitial N doping.[54] Hence, the present composite CuCoNT NFs, there may be also possible of Cu – O – N, Co – O – N linkages. The very keen point is that both substitutional and interstitial N doping is occurred in the composite CuCoNT NFs. But the involvement of substitutional N doping is more than interstitial. An efficient substitutional N doping is due to the availability more oxygen form TiO_2, CuO and Co_3O_4 in the composite CuCoNT NFs. Moreover, the binding energy of ca. 396 eV is ascribed as β-N and can be attributed to Ti – N interaction.[51,555] It has been noted that the binding energy located at ca. 459.1 and 464.8 eV for peaks Ti $2p_{3/2}$ and Ti $2p_{1/2,}$ respectively, are due to the presence of Ti^{4+} in the pure TiO_2 lattice.[56] In the present investigation (Figure 6b), it appeared at ca. 457.5 eV (Ti $2p_{3/2}$) and at ca. 463.1 eV (Ti $2p_{1/2}$). The low BE of TiO_2 is due to the transfer of electron from N to Ti (forming Ti^{3+}) and the transfer of electron from O to Ti, since O is electronegative and Ti is electropositive. The other factor is the electron may also transfer from O atom (CuO and Co_3O_4) to Ti. These are the main reason to high reduction Ti^{4+} to Ti^{3+} in the composite CuCoNT NFs which leads to shift to the visible light region.

The XPS spectrum of neat CuO NFs is investigated in Figure S7. The main peaks are at ca. 933.3 eV (Cu $2p_{3/2}$) and 953.1 eV (Cu $2p_{1/2}$), along with the presence of their characteristic shakeup satellite peaks are at ca. 941, 943.1 and 961.6 eV, respectively, are due to the existence of pure CuO. This result is consistent with Hou et al. investigation.[57] In composite CuCoNT NFs (Figure 6c), the BE of Cu $2p_{3/2}$ and Cu $2p_{1/2}$ is at ca. 934 and 953.86 eV, along with two satellite peaks are at ca. 942 and 962.3 eV, indicating fully oxidized CuO in composite CuCoNT NFs.[58] As CuO is oxidized in the composite, the electron movements are favorable. That's why the higher shifting of CuO BE (CuCoNT NF) is occurred by transferring the electron from Cu^{2+} to Ti^{4+}. The possible bond linkage will be Cu – Ti – O – N. Moreover, the BE of pure Co_3O_4 NFs (Figure S7) are located at ca.778.8 and 794.5 eV can be assigned to Co $2p_{3/2}$ and Co $2p_{1/2}$, respectively, along with weak satellite peaks are located at higher binding energy side. The present XPS analyses for neat Co_3O_4 NFs is similar with the the signature spectrum of Co_3O_4.[59,60] Figure 6d, the Co $2p_{3/2}$, Co $2p_{1/2}$ and two satellites peaks are observed at ca. 780.93, 796.2, 786.7 and 803.4 eV, respectively.These high shifts of BE of Co_3O_4 in CuCoNT NFs as compared to neat Co_3O_4 is may be due to the transfer of electron from Co^{2+}/Co^{3+} to Ti^{4+} and forming the Co – Ti – O – N linkage. The high BE shiftig of Co $2p_{3/2}$ in neat Co_3O_4 NFs (778.8 eV) to Co_3O_4 in composite CuCoNT NFs (780.93 eV) is due to the strong electronic interacton Co^{2+}/Co^{3+} to Ti^{4+}. This is the reason that N-type TiO_2 preferbly mixed with P-type Co_3O_4 and formed p-n heterojunction, whereas CuO act as cocatalyst. It is observed that the peak at the binding energy of O1s ca. 529.3 eV is signified to Ti – O and Cu – O species.[57] The O 1s BE in composite CuCoNT NFs (Figure 6e) is observed at ca. 528.90 eV is due to the strong interaction of O with Ti, Cu, Co in the form of Ti – O, Cu – O and Co – O, respectively. Conclusively, the composite CuCoNT NFs might be consists of – Cu – Co – Ti – O – N – and – Cu – O – Co – O – Ti – N – linkages.

The FTIR spectra of TiO_2 NFs, NT NFs, composite CoNT NFs, CuNT NFs and CuCoNT NFs are displayed in the Figure S8. The bands at 3420 and 1640 cm^{-1} are attributed to the stretching vibration of –OH groups for all nanofibers. For all samples, the peak at 2342 cm^{-1} is due to the adsorbed CO_2 gas. This adsobed CO_2 gas is an instrumental error and created during analysis. All the samples represent a broad bands in between 479 to 633 cm^{-1}, are assigned to the stretching vibration of Ti–O and bridging stretching modes Ti–O–Ti.[61] This is because all samples are containing TiO_2 NFs and oxide modified N-TiO_2 NFs. The weak peak at 1393 cm^{-1} in the spectrum of the NT NFs, is assigned to the vibrations of N–H bonds.[62] This peak is not clearly visible for other samples are due to the modification of CuO and Co_3O_4 within NT NFs. The Cu – O stretching vibration is observed in between 489 to 533 cm^{-1} is due to the formation of CuO within N – TiO_2 NFs (CuNT NFs).[63] The broad peak from 572 to 645 cm^{-1} is observed for the formation of Co_3O_4 in N – TiO_2 NFs (CoNT NFs).[64] The formation of CuO and Co_3O_4 within NT NFs (CuCoNT NFs) is observed due the presence of a broad peak at 469 – 648 cm^{-1}.[63,64]

2.6 Formation mechanism of composite CuCoNT NFs

The possible formation mechanism of mesoporous composite CuCoNT NFs is explained on the basis aforesaid experiments, which are illustrated in the Scheme 1. The composite CuCoNT NFs are fabricated on the basis of *in situ* sol – gel electrospinning method. The *in situ* process is the phenomenon where the entire reacting precursors are involved in reaction in the same place without isolating to the other system. The present fabrication process is occurred in the one pot synthesis, which termed as *in situ* process. Sol – gel process is nothing but a process of hydrolysis and condensation. Firstly, nucleation of sol particles is observed when metal solutions are hydrolyzed. The generated Ti $(OH)_4$ sol particles will combine the metal ions such as Cu^{2+} and Co^{2+} through oxygen atom along with nitrogen through electrostatic interaction,resulting Cu – N – Ti – O – Co bond. The hydroxyl groups of respective metals are combining with PVP and PEG. The formation of hydrogen bonding occurred between C=O groups of PVP and –OH groups of $Ti(OH)_4$, Co $(OH)_2$ and $Cu(OH)_2$. The hydrophilicity nature of PEG is also thermodynamically favorable for hydrogen bonding with $Ti(OH)_4$, $Co(OH)_2$ and $Cu(OH)_2$.The hydrogen bonding is also occurred in –O– group of PEG with –OH groups of $Ti(OH)_4$, $Co(OH)_2$ and $Cu(OH)_2$. PVP and PEG were dissolved after long time reaction and forming polymer chain around the sol. The acetic acid was used as a sol stabilizer. This is due to that acetic acid has ability to retard the condensation

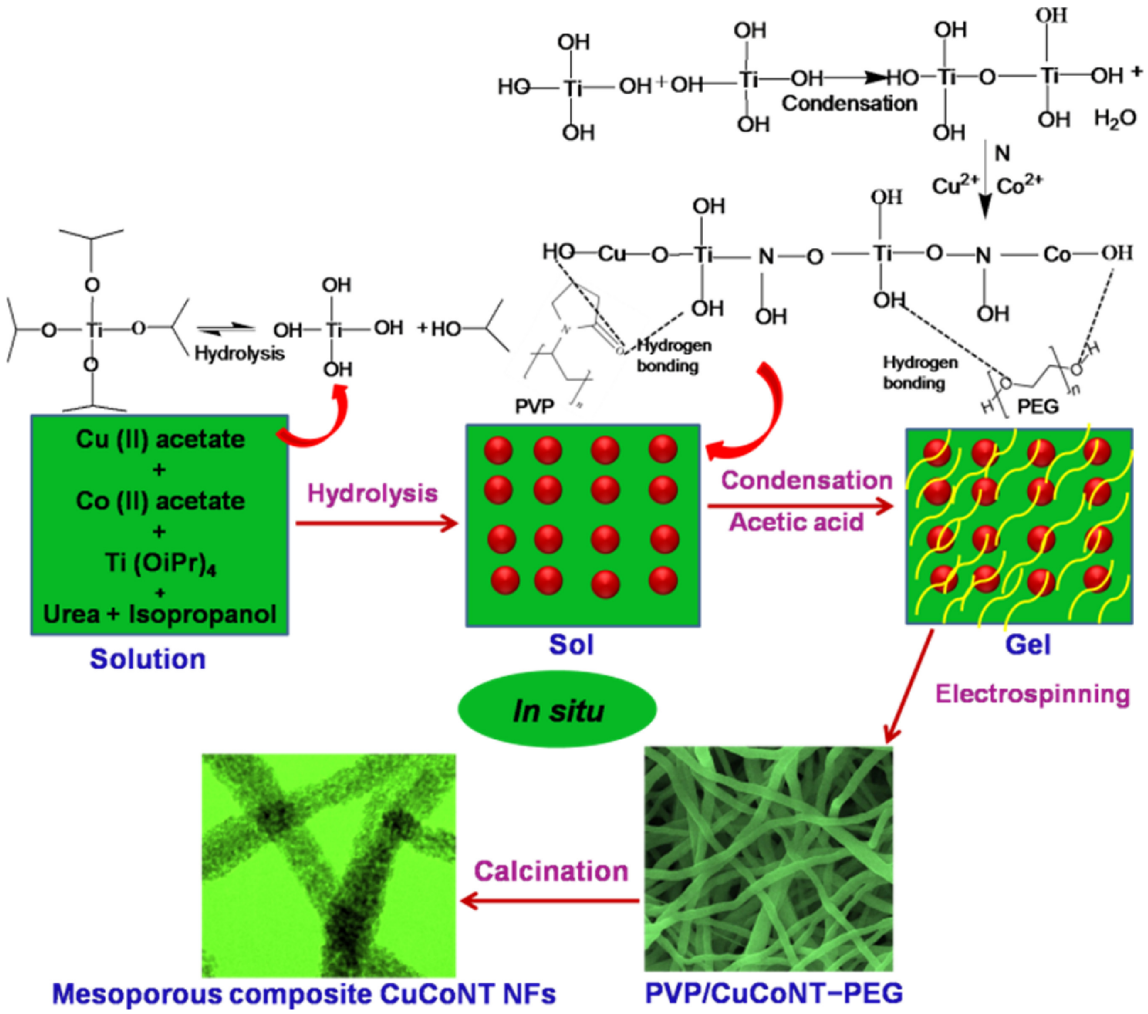

Scheme 1. Schematic diagram of formation mechanism of mesoporous composite CuCoNT NFs.

and slowing the gelation rate of sol.[65] The sol starts to get gel by applied electric current while introduce in electrospinning chamber. The resulted, smooth PVP/CuCoNT – PEG nanofibers are formed by dried in 70 °C. The fibrous morphology is due to the supramolecular arrangement of linear structure of both PVP and PEG. The mesoporous composite CuCoNT NFs are formed by calcination at 450 °C for 4 h i.e. removal of PVP and PEG. The mesoporous/rough morphology formed by quick evaporation/degradation of low molecular weight PEG and NFs are formed due to the decomposition of linear structure PVP.

2.7 Visible light photocatalytic activity of NFs

Fabricated electrospun NFs have potential photocatalytic activity toward the mixed dyes of methylene blue (MB) and methyl orange (MO) (MB + MO) degradation in visible light. It was observed that mesoporous composite CuCoNT NFs has high photocatalytic activity of mixed dyes degradation than other NFs. The reaction was carried out for 60 min in the presence of visible light, 30 mg.L^{-1} of mixed dyes, and 1 mg.ml^{-1} of catalyst. The pH of the solution has a vital role for degradation of mixed dyes. The pH is the most important factor affecting the photocatalytic degradation process. The effect of pH on the degradation of mixed dyes (MB + MO) is shown in Figure S9. The experiment was performed at pH values of 4, 6, 8, and 10 by using mesoporous composite CuCoNT NFs as photocatalyst. It is observed that the degradation of mixed dyes was 100% at pH 10. It has also been observed that at alkaline pH, the generation of hydroxyl radicals are favored by the formation of hydroxide species.[9] Moreover, it has also been reported that at alkaline pH the generation of •OH radicals is more than that at acidic pH.[66] Hence, the generated hydroxyl radicals (•OH) are played a key role in the degradation of mixed dyes at pH 10.The photocatalytic degradation of mixed dyes by different NFs is shown in Figure 7a. The reaction was carried out in the presence of visible light at pH 10 in 60 minute. The intensity of UV-Visible absorbance spectra is decreases gradually from TiO_2 NFs to CuCoNT NFs. The least absorbance intensity for mesoporous composite CuCoNT NFs, indicating high degradation of mixed dyes. The high degradation activity of mesoporous composite CuCoNT NFs is due to the efficient visible light absorption

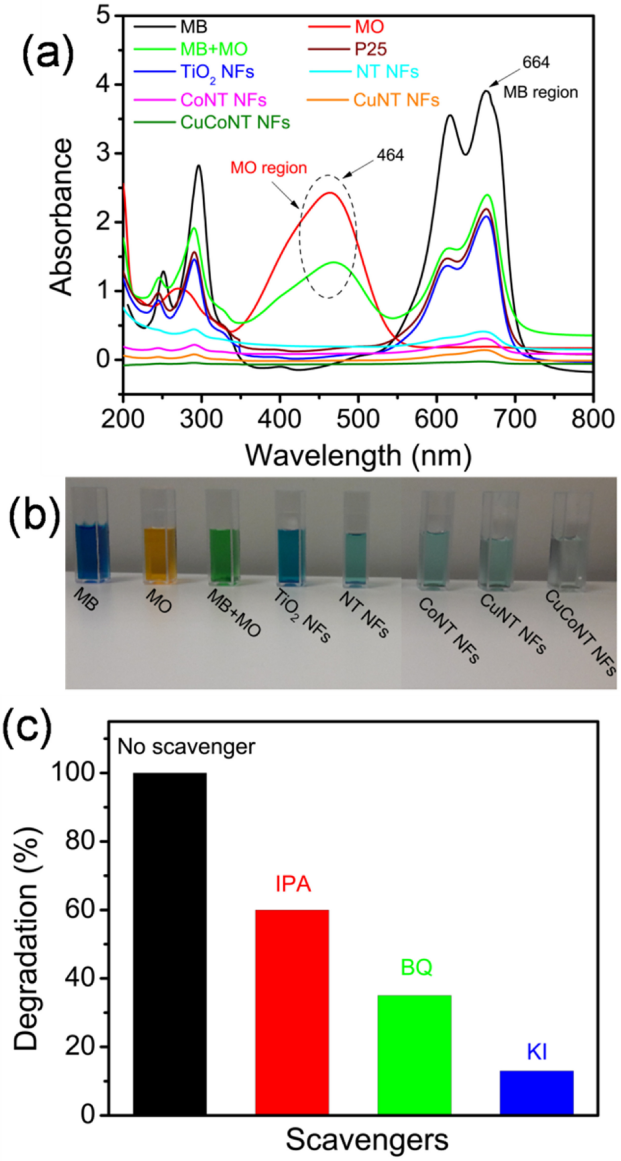

Figure 7. (a) UV-Vis spectra of the solution recorded after photocatalytic degradation of mixed methylene blue and methyl orange (MB + MO). The absorbance of standard solutions (MB, MO and MB + MO) and the reaction solutions (after degradation by catalyst) are not diluted in the measurement time. The degradation process is carried out by using different 5 mg of catalyst in a 5 ml (MB + MO) solution at pH 10 in visible light for 60 minute, (b) color change after degradation mixed dyed by different catalysts, (c) Results of reacting species trapping experiments performed by using IPA, BQ and KI on composite CuCoNT NFs.

property of CuCoNT NFs. The less mixed dyes degradation ability by TiO_2 NFs and least degradation ability of P25 is due to the least visible light absorption property. The % of degradation is calculated from absorbance of mixed dyes solutions after degradation by different NFs,which is shown in the Table S2. The photocatalytic performance exhibited the following trend: P25 < TiO_2 NFs < NT NFs < CoNT NFs < CuNT NFs < CuCoNT NFs. The degradation % of TiO_2 NFs is higher than that of P25, which is due to the NFs morphology and mesoporous framework. These structural properties of TiO_2 NFs enhance surface active sites for the degradation of the mixed dyes. Figure 7b shows that the MB + MO (mixed dyes) color changes when reacting with different catalysts. The blue, orange and green colors are corresponding to the standard of MB, MO and MB + MO, respectively. The degradation reaction is performed only in mixed dyes, i.e. green color. The concentration of green color for mixed dyes decreases from TiO_2 NFs to CuCoNT NFs. The result shows that after degradation orange color of MO disappeared quickly and blue color of MB left upto CuNT NFs. The quick disappearance of MO is due to the strong columbic attraction of negative charge MO^- with positive charge MB^+. This is the vital finding for degradation of multiple dyes simultaneously.

In order to check the active species involved in the quick photocatalytic mixed dyes degradation, trapping experiments of active species during the photocatalytic performance of composite CuCoNT NFs under visible irradiation are shown in the Figure 7c. It has been well-known that the photogenerated holes (h^+), hydroxyl radicals ($^{\bullet}OH$) and superoxideradicals ($O_2^{\bullet -}$) are treated as the vital reactive species involved in photodegradation reactions. As shown in the Figure 7c, the photocatalytic degradation of mixed dyes decreased drastically when KI is used as scavenger. That means the photogenerated holes (h^+) are the major reactive species for the degradation of mixed dyes. When IPA is used as scavenger, the mixed dyes degradation decreased very less as compared to reaction performed without scavenger, indicating least involvement of $^{\bullet}OH$ species in the overall degradation process. The degradation of mixed dyes is significant when BQ used as $O_2^{\bullet -}$ scavanger, indicating small involvement of $O_2^{\bullet -}$ species in the reaction. Hence, it is concluded that h^+ and $O_2^{\bullet -}$species plays an important role for the degradation of mixed dyes in the visible light. The high involvements of h^+ in the reaction media are indicating effective separation of photogenerated electron and hole.

The kinetics study of mixed dyes degradation by photocatalytic process on mesoporous composite CuCoNT NFs is shown in Figure S10. The plot is plotted between log C_0/C vs t. The kinetic study was performed by varying the concentration of mixed dyes (30, 40 and 50 mg. L^{-1}) with time (20, 40 and 60 min) at different pH (4, 6, 8 and 10). With increase in the concentration of mixed dyes at different pH, the degradation decreases. A linear relationship is observed between concentrations of mixed dyes with irradiation time at different pH. The photocatalytic degradation of mixed dyes are followed the first order kinetics. The data is fitted well to the first order rate model and the equations (2) and (3) are given below.

$$log\frac{C_0}{C} = Kt/2.303 \quad (2)$$

$$K = (log\frac{C_0}{C} \times 2.303)/t \quad (3)$$

Where K is the first order rate constant, C_0 is the initial concentration of mixed dyes and C is the concentration at time t.

2.7.1 Mechanism of mixed dyed degradation by mesoporous composite CuCoNT NFs

For constructing perfect heterostructures, considering the suitable conduction band (CB) and valence band (VB) levels of the two individual semiconductors is necessary. This will gives idea about the increment in photocatalytic activity of the designed photocatalyst. The conduction band (E_{CB}) edge N-TiO_2 and Co_3O_4 can be calculated by equation 4.[67]

$$ECB = X - EC - 0.5(Eg) \quad (4)$$

Where X is the absolute electronegativity of semiconductor which is calculated from the absolute electronegativity of the constituent atoms, $E_C = \sim 4.5$ eV (energy of free electrons measured on the hydrogen scale) and E_g is the band gap of the semiconductor. The VB edge (E_{VB}) can be determined by.The band edge diagram of both semiconductors is shown in the Scheme 2. Sheme 2 shows that the calculated value of E_{CB} and

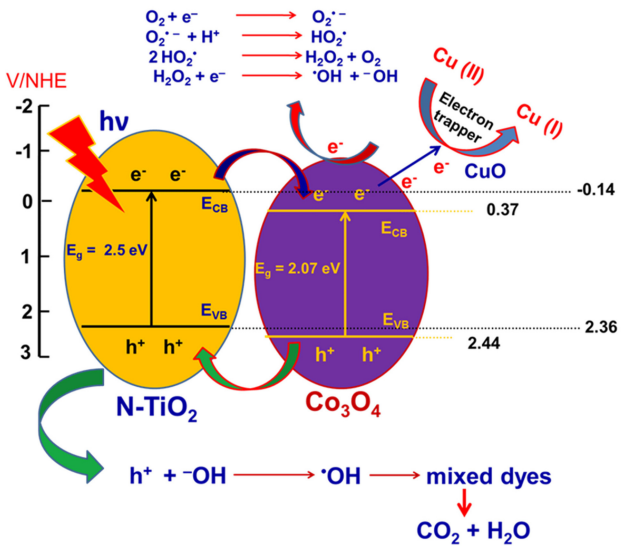

Scheme 2. Schematic diagram of the separation and electron – hole transfer in composite CuCoNT NFs along with the possible reaction mechanism.

E_{VB} in N-TiO_2 is – 0.14 eV and 2.36 eV, respectively. Likewise, the E_{CB} and E_{VB} values of Co_3O_4 are 0.37 and 2.44 eV, respectively. As the position of E_{CB} for Co_3O_4 is more positive than N-TiO_2, hence the photo- generated electrons can transfer easily from E_{CB} of N-TiO_2 to E_{CB} of Co_3O_4.[68] Moreover, the photogenerated hole (h^+) will transfer from valence band (E_{VB}) edge of Co_3O_4 to E_{VB} of N-TiO_2. Thus, N-TiO_2 and Co_3O_4 have the suitable conduction and valence band edge for endorsing charge separation at the heterojunction interfaces. But still there may be possible of e^- and h^+ recombination. In order to overcome this problem, an electron trap center like CuO (cocatalyst) will help for trapping extra electrons, which leads to suppress the electron – hole recombination efficiently. Katsumata et al. have observed that CuO has four electron reduction ability.[69] This is due to the high reducibility nature of Cu(II) in CuO, leads to trapping of electrons.This phenomenon helps to suppress the electron – holes recombination and makes CuO as an effective cocatalyst. This is the vital reason that CuCoNT NFs shows higher mixed dyes degradation in visible light as compared to other NFs (Figure 7a). The degradation mechanism of mixed dyes is occurred by influence of electron and hole (Scheme 2). The photogenerated electrons are reacting with surface molecular oxygen generating active species such as $O_2^{\bullet -}$, $HO_2^{\bullet -}$ and •OH. As per the trapping reaction (Figure 7c), the significant role of $O_2^{\bullet -}$ in photocatlytic process is also helped to suppress the electron hole recombination. This is because electrons are utilized to reduced the surface O_2 to $O_2^{\bullet -}$. These oxidizing species are responsible for oxidized/decompose the mixed dyes. Another way, the •OH radical is formed when hole is reacting with $^-$OH, leads to oxidized/decompose the mixed dyes, resulting degrade products CO_2 and H_2O. Thus, the charge separation and degradation mechanism have been well established in visible light.

2.7.2 Factor affecting the photocatalytic activity

The degradation of mixed dyes (MB + MO) has been achieved by (a) the role of mesoporous NFs morphology, (b) lowering of electron – hole recombination, generation of oxygen vacancies and photocurrent measurement, and (c) role of cocatalyst

2.7.2.1 Role of mesoporous nature of NFs

Mesoporous nanofibers have great deal of importance in the field of catalysis. This is because it will act as an efficient catalyst because of high surface to volume ratio. The SEM study depicts that the size of NFs diameter of all samples are below 100 nm, which leads to high surface area. Another thing is that if the NFs are in mesoporous nature, i.e. mesoporous NFs, then the surface area increases as compared to neat NFs. These properties of materials help to increase the greater active site for the accommodation of a substrate mixed dyes molecule. It has been also observed from HR-TEM image that the NFs are in mesoporous nature. The mesoporosity and NFs morphology of all materials will acquire high surface area, leads to high and swift mixed dyes degradation activity in visible light. The high photocatalytic activity of composite CuCuNT NFs as compared to other NFs, is may be due to the generation of high surface hydroxyl groups. The formation of high surface hydroxyl groups may be due to the presence more metal oxide centers such as CuO and Co_3O_4 within N-TiO_2 (composite CuCuNT NFs). The highly reactive hydroxyl radicals (•OH) are formed form surface hydroxyl groups by absorbing visible light. This process may makes the composite CuCoNT NFs as an efficient photocatalyst towards mixed dyes degradation in visible light.

2.7.2.2 Lowering of electron-hole recombination, generation of oxygen vacancies and photocurrent measurement

The efficiency of charge carrier trapping, immigration, and transfer behaviors of the photoexcited electron–hole pairs in

semiconductors has been investigated by photoluminescence (PL) emission.[70] A comparison of the PL emission (λ_{exc} = 390 nm) spectra of pure TiO_2 NFs, NT NFs and composite NT NFs are shown in Figure 8a. The PL intensities of the NT NFs

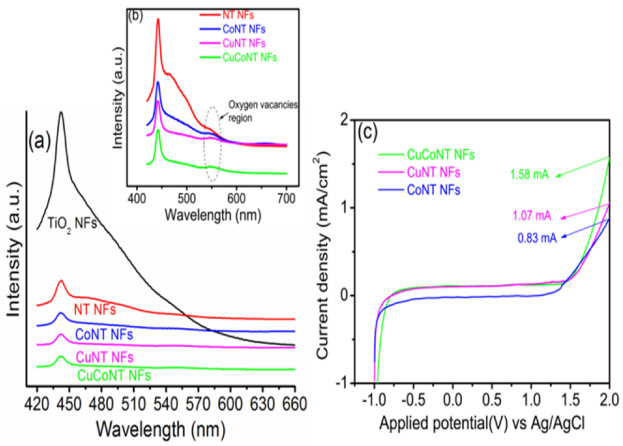

Figure 8. (a) Photoluminescence spectra of different NFs photocatalysts, (b) evolution of oxygen vacancies in NT NFs, CoNT NFs, CuNT NFs and CuCoNT NFs (in set) and (c) Photocurrent and potential curves are obtained under visiblelight illumination of mesoporous CoNT NFs, CuNT NFs and CuCoNT NFs.

and semiconductor composite NT NFs are consistently lower than that of pure TiO_2 NFs. Under light irradiation, the PL emission describes the recombination of excited electrons and holes. Hence, the lower PL intensity indicates a lower recombination rate of electron–hole.[70] The lowest recombination of electron-hole favors the highest photocatalytic activity. Presently, the composite CuCoNT NFs has lowest electron – hole recombination as compared to pure TiO_2 NFs, NT NFs and other composite NT NFs which is indicating highest photocatalytic activity of mixed dyes degradation. The lowest electron – hole recombination of composite CuCoNT NFs is due to the formation of (i) oxygen vacancies and (ii) creation of Schottky barrier at CuO, Co_3O_4 and N-TiO_2 interface.[71] The oxygen vacancies of nanofibers are pictured in the Figure 8b (inset). Expect TiO_2 NFs (Figure 8a), the NT NFs and other semiconductor composite NT NFs showing oxygen vacancies at 548 nm. This is due to the interstitial/substitutional doping of nitrogen into the TiO_2, resulting formation of Ti^{3+}. The Ti^{3+} aids to trap the photoemission electron from conduction band of TiO_2 via non radiative transition. This phenomenon prevents the electron – hole recombination and resulting swift photocatalytic degradation of mixed dyes in visible light. Furthermore, the Schottky barrier appears due to the mixing of the CuO and Co_3O_4 into the N-TiO_2. This phenomenon helps to create superficial space charge layer between valence and conduction band of TiO_2, which could act as an electron sink efficiently prevent the electron – hole recombination.[72,73] That's why PL intensity gradually decreases from NT NF > CoNT NFs > CuNT NFs > CuCoNT NFs. Conclusively, the doping of nitrogen creating oxygen vacancies and mixing of CuO and Co_3O_4 (CuCoNT NFs) generating schottky barriers.

The photocurrent measurement of mesoporous CoNT NFs, CuNT NFs and composite CuCoNT NFs is carried out in visible light in order to correlate the photoelectrochemical properties with the photocatalytic activity of the fabricated nanofibers (Figure 8c). A photocurrent generation in the anodic direction was observed under irradiation of light ($\lambda \geq 400$ nm). The photocurrent of NFs photocatalysts is increased with positive applied bias which shows their n-type semiconducting property. The photocurrent density of mesoporous CoNT NFs, CuNT NFs and composite CuCoNT NFs is found to be 0.83 and 1.07 and 1.58 mA/cm^2, respectively. The increased photocurrent in all mesoporous NFs photocatalysts may be due to the mesoporosity, nanofibers morphology, high surface area and high light absorption property. It has observed that the photocurrent density of mesoporous composite CuCoNT NFs is higher than that of CoNT NFs, CuNT NFs. This indicates that a larger number of free electrons are transported in the circuit in the case of the mesoporous composite CuCoNT NFs photoelectrode. Here CuO as a cocatalyst in composite CuCoNT NFs possesses an outstanding ability to sink the photogenerated electron and transport it on its surface and hence, reduces the recombination rate of electron – hole pairs. This obtained results from the photoelectrochemical behavior of mesoporous composite CuCoNT NFs is in good agreement with PL studies. The combotorial effect of PL studies, oxygen vacancies and photocurrent mesurements aids to lowering the electron – hole recombination which resulting high mixed dyes degradation in visible light by mesoporous composite CuCoNT NFs than other presently fabricated NFs.

2.7.2.3 Role of CuO as cocatalyst in mesoporous composite CuCoNT NFs

The lowest PL spectrum of mesoporous composite CuCoNT NFs, signifies the vital role of CuO for high degradation of mixed dyes. It has been also seen that even composite CuNT NFs has not that much of degradation ability. Hence, combination of CuO, Co_3O_4 and N-TiO_2 in CuCoNT NFs has important role, which made CuO a cocatalyst. As a cocatalyst, CuO enhances the photocatalytic activity of mesoporous composite CuCoNT NFs by a two way action: (i) by absorbing the photoexcited electrons, as an electron trapper, which leads to suppress of electron – hole recombination. This phenomenon facilitates the separate involvement of electron and hole for degradation mixed dyes in visible light. Qui et al. observed that pure CuO i.e. Cu (II) is photocatalytically inactive; however, Cu(II) species in nanoclusters are very efficient for the visible light photo catalysis of TiO_2.[74] Hence, in the present study mixing of CuO in nanofibrous framework of composite CuCoNT NFs facilitate the efficient photcatalytic mixed dyes degradation in visible light. (ii) trapping of electrons by Cu (II) center of CuO and reduced to Cu (I) in CuCoNT NFs.This process is also helps to suppress the electron – hole recombination and enhanced the visible light response mixed dyes degradation. Hence, role

of CuO as low cost cocatalyst for proficient mixed dyes degradation in visible light is well-established.

2.7.3 Evidence, stability and versatility of organic pollutant degradation

In order to check the complete mineralization of mixed dyes (MB + MO) after degradation, the FTIR spectra of pure CuCoNT NFs, degradation of mixed dyes (MB + MO) on CuCoNT NFs and pure mixed dyes (MB + MO) have been done (Figure 9a). In

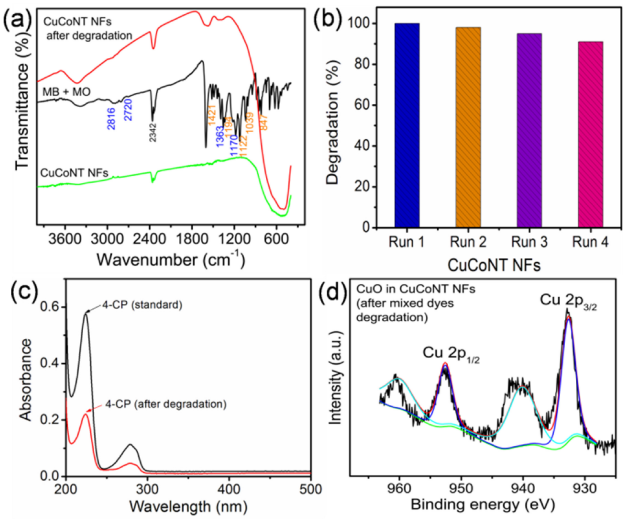

Figure 9. (a) FTIR spectra of pure CuCoNT NFs, MB + MO and CuCoNT NFs (after degradation). (b) Recycling study of mixed dyes (MB + MO) degradation by CuCoNT NFs, (c) UV-Visible spectra of 4-Chlorophenol (4-CP) degradation by CuCoNT NFs. The degradation reaction is performed by taking 5 mg of CuCoNT NFs in 5 ml 4-CP solution in visible light for 60 minute. (d) Core shell XPS spectrum of CuO in composite CuCoNT NFs after mixed dyes degradation.

pure MB + MO, the signature peaks of both MB and MO are seen in blue and orange color, respectively. The blue color peaks 2816, 2720, 1363 and 1170 cm^{-1} are assigned to the stretching vibration of -CH- aromatic ring, $-CH_3$ methyl groups, aromatic ring structures and C=C skeleton aromatic ring structures in methylene blue, respectively.[75] The MO signature peaks (orange color) 1421, 1194 and1122 cm^{-1} are assigned to the N=N vibration, C – N vibration and S=O vibration, respectively. The peaks 1039 and 847 cm^{-1} are due to the C–H stretching vibrations of the benzene ring of MO.[76] The weak bands are also visible in the range of 600–800 cm^{-1} and are may associated with the out-of-plane bending mode of C–H or O–H groups. For all samples, the peak at 2342 cm^{-1} is an instrumental error for adsorbed CO_2 gas. The signature peaks of MB + MO are absent in composite CuCoNT NFs after degradation, indicating the complete mineralization of MB + MO during reaction. The FTIR spectrum of pure composite CuCoNT NFs is shown Figure 9a for comparison.

The stability study regarding mixed dyes degradation by composite CuCoNT NFs is shown in Figure 9b. The reaction was evaluated by performing recycling experiments on the mixed dyes degradation under similar conditions. The activity was found to be almost same in three repeated runs and then there is slight decrease in the activity. In order to check the versatile nature of mesoporous composite CuCoNT NFs, the degradation of 4-CP (30 $mg.L^{-1}$) has been performed (Figure 9c). It is calculated that 63% 4-CP degradation achieved only 60 minute. This percentage of degradation is calculated by the decrease in UV-Visible absorbance of 4-CP after reaction. The 4-CP degradation achievement is due to the efficient visible light absorption by composite CuCoNT NFs. The highly reactive $^{\bullet}OH$ radical is formed followed by generation of electron – hole which leads to degradation of 4-CP to H_2O and CO_2. In order to compare the 4-CP degradation with mixed dyes degradation, the reaction conditions like concentration, amount of catalyst, time duration is kept similar like mixed dyes. The most exciting achievement is that mesoporous composite CuCoNT NFs shows high photocatalytic activity towards colorless 4-CP degradation in visible light. Hence, mesoporous composite CuCoNT NFs is not merely an efficient visible light photocatalyst for degradation of mixed dyes (100%) but also colorless 4-CP (63%) in 60 minute.

In order to check the formation of Cu_2O i.e. Cu(I) after degradation of mixed dyes, the XPS analyses of composite CuCuNT NFs has been done after degradation. The XPS spectrum of CuO in composite CuCoNT NFs (after mixed dyes degradation) is shown in the Figure 9d. The main peaks are at ca. 932.54 eV (Cu $2p_{3/2}$) and 952.1 eV (Cu $2p_{1/2}$) are due to presence of Cu_2O which is consistent with the Thir et al. results.[77] The presence of satellite peaks indicates the presence of CuO. Hence, after degradation some part of CuO {Cu (II)} may be reduced to Cu_2O (Cu^+) by trapping photogenerated electrons, which enables the efficient photocatalysis properties by reducing electron–hole recombination.

3. Conclusions

The vital conclusion of the present study is the successful fabrication of mesoporous TiO_2 NFs, NT NFs, CoNT NFs, CuNT NFs and CuCoNT NFs by *in situ* sol – gel electrospinning method. The role of PVP and PEG as polymeric matrix for the electrospinning of mesoporous and NFs morphology of all samples are well-established, newness of the present investigation. The low and high molecular weight of polymers, hydrogen bonding between polymers and metal hydroxide and hydrophilicity of PEG are responsible for formation of mesoporous nanofibers. Mesoporous composite CuCoNT NFs shows highest (100%) photocatalytic mixed dyes degradation as compared to other photocatlysts (TiO_2 NFs, NT NFs, CoNT NFs, CuNT NFs and P25) in visible light. The photocatalyst CuCoNT NFs is stable upto 4th runs and there is minimal change in degradation activity, proved by stability test. The most interesting part is that the complete mineralization of mixed dyes molecules is occurred after degradation, examined by FTIR study. That means photocatalyst will be stable, reactive and reusable for multiple runs. The high and swift photocatalytic activity by mesoporous composite CuCoNT NFs is ascribed to

the role of low cost CuO as cocatalyst in visible light. The electrons trap property of CuO in composite enhances the visible light degradation of mixed dyes. The versatility of composite CuCoNT NFs has been well-established by degrading 63% 4-CP in 60 minute.Moreover, (a) mesoporous and nanofibers morphology of photocatalysts, (b) formation of oxygen vacancies, (c) lowering of electro – hole recombination and (d) high photocurrent response, are the key factors which make mesoporous composite CuCoNT NFs as an efficient versatile visible light active photocatalyst for degradation of organic pollutants such as textile dyes (i.e. methylene blue and methyl orange) and phenolic compounds (i.e. 4-chlorophenol).

Supporting information summary

Table summarizing textural properties of mesoporous NFs,SEM picture of PVP/CuNT – PEG and CuNT NFs and PVP/CoNT – PEG, CoNT NFs,TEM and HRTEM micrographs of composite CuNT NFs and CoNT NFs, SAED pattern of all mesoporous NFs, STEM-EDAX elements mapping of CuCoNT NFs, STEM-EDX spectra of TiO_2 NFs, NT NFs and composite CuCoNT NFs. XPS spectra of neat CuO NFs and Co_3O_4 NFs FTIR spectra of all mesoporous NFs, effect of pH on mixed dyes (MB + MO) degradation by mesoporous composite CuCoNT NFs, reaction kinetics of mixed dyes degradation by CuCoNT NFs at different pH, and table shows the % of mixed dyes degradation by different NFs.

Acknowledgements

A. C. Pradhan acknowledges The Scientific & Technological Research Council of Turkey (TUBITAK), BIDEB 2216-Fellowships for Research Fellowship Programme for Foreign Citizens) for postdoctoral fellowship. A. Senthamizhan acknowledges TUBITAKBIDEB 2221 fellowship program for visiting scientists. T. Uyar acknowledges The Turkish Academy of Sciences - Outstanding Young Scientists Award Program (TUBA-GEBIP)-Turkey for partial funding. Authors also thank M. Guler for TEM-STEM technical support.

Conflict of Interest

The authors declare no conflict of interest.

Keywords: Dye Degradation · Electrospinning · Nanofibers · TiO_2 · Visible Light Photocatalysis

[1] K. R. Reddy, M. Hassan, V. G. Gomes, *Appl. Catal. A: General* **2015**, *489*,1–16.
[2] A. Meng, J. Zhang, D. Xu, B. Cheng, J. Yu, *App. Catal. B: Environ.* **2016**, *198*, 286–294
[3] A. C. Pradhan, B. Nanda, K. M. Parida, G. R. Rao, *J. Phys. Chem. C* **2015**, *119*, 14145–14159.
[4] F. Kayaci, S. Vempati, C. Ozgit-Akguna, I. Donmez, N. Biyikli, T. Uyar, *Appl.Catal. B: Environ* **2015**, *176–177*, 646–653.
[5] A. Senthamizhan, B. Balusamy, Z. Aytacab, T. Uyar, *CrystEngComm* **2016**, *18*, 6341–6351.
[6] K. R. Reddy, K. V. Karthik, S. B. B. Prasad, S. K. Soni, H. M. Jeong, A. V. Raghu, *Polyhedron* **2016**, *120*, 169–174.
[7] A. C. Pradhan, M. K. Sahoo, S. Bellamkonda, K. M. Parida, G. R. Rao, *RSC Adv.* **2016**, *6*, 94263–94277.
[8] L. Tang, J.-j. Wang, L. Wang, C. Jia, G. Lv, N. Liu, M. Wu, *ACS Sustainable Chem. Eng.* **2016**, *4*, 4617–4625.
[9] B. Nanda, A. C. Pradhan, K. M. Parida, *Micropor. Mesopor. Mater.* **2016**, *226*, 229–242.
[10] G. Zhang, L. Qin, L. Chen, Z. Xu, M. Liu, X. Guo, *ChemCatChem* **2016**, *8*, 426–433.
[11] J. Yu, J. Ran, *Energy Environ. Sci.* **2011**, *4*, 1364–1371
[12] K. R. Reddy, K. Nakata, T. Ochiai, T. Murakami, D. A Tryk, A. Fujishim, *J. Nanosci. Nanotechnol.* **2011**, *11*, 3692–3695.
[13] D. Zhou, Z. Chen, Q. Yang, C. Shen, G. Tang, S. Zhao, J. Zhang, D. Chen, Q. Wei, X. Dong, *ChemCatChem* **2016**, *8*, 3064–3073.
[14] N. Chitpong, S. M. Husson, *J. Membrane Sci.* **2017**, *523*, 418–429.
[15] A.Md Showkat, Y.-P. Zhang, M. S. Kim, A. I. Gopalan, K. R. Reddy, K.-P. Lee, *Bull. Korean Chem. Soc.* 2007, 28,1985–1992.
[16] Y. Liu, L. Zhao, M. Li, L, Guo, *Nanoscale* **2014**, *6*, 7397–7404.
[17] K. Zhu, N. R. Neale, A. Miedaner, A. J. Frank, *Nano Lett.* **2007**, *7*, 69–74.
[18] N. Qin, Y. Liu, W. Wu, L. Shen, X. Chen, Z. Li, L. Wu, *Langmuir* **2015**, *31*, 1203–1209.
[19] Z. Zhang, C. Shao, X. Li, Y. Sun, M. Zhang, J. Mu, P. Zhang, Z. Guo, Y. Liu, *Nanoscale* **2013**, *5*, 606 – 618.
[20] L. Nie, J. Yu, J. Fu, *ChemCatChem* **2014**, *6*, 1983–1989.
[21] K. R. Reddy, K. Nakata, T. Ochiai, T. Murakami, D. A. Tryk, A. Fujishima, *J. Nanosci. Nanotechnol.* **2010**, *10*, 7951–7957.
[22] X. Wang, J. Choi, D. R. G. Mitchell, Y. B. Truong, I. L. Kyratzis, R. A. Caruso, *ChemCatChem* **2013**, *5*, 2646–2654.
[23] A. Abdal-hay, A. S. H. Makhlouf, H. K. A. Khalil, *ACS Appl. Mater. Interfaces* **2015**, *7*, 13329–13341.
[24] S. K. Choi, S. Kim, S. K. Lim, H. Park, *J. Phys. Chem. C* **2010**, *114,* 16475–16480.
[25] C. Wessel, R. Ostermann, R. Dersch, B. M. Smarsly, *J. Phys. Chem. C* **2011**,*115*, 362–372.
[26] S. Zhan, D. Chen, X. Jiao, C. Tao, *J. Phys. Chem. B* **2006**, *110*, 11199–11204.
[27] K. Tanaka, F. V. M. Capule, T. Hisanaga, *Chem. Phys. Lett.* **1991**, *187*, 73–76.
[28] R. Asahi, T. Morikawa, T. Ohwaki, K. Aoki, Y. Taga, *Science* **2001**, *293*, 269–271.
[29] S. U. M. Khan, M. Al-Shahry, W. B. Ingler, *Science* **2002**, *5590*, 2243–2245.
[30] J. Fang, F. Wang, K. Qian, H. Bao, Z. Jiang, W. Huang, *J. Phys. Chem. C*, **2008**, *112*, 18150–18156.
[31] Z. Luo, H. Jiang, D. Li, L. Hu, W. Geng, P. Wei, P. Ouyang, *RSC Adv.* **2014**, *4*, 17797–17804.
[32] W. Z. Wang, X. W. Huang, S. Wu, Y. X. Zhou, L. J. Wang, H. L. Shi, Y. J. Liang, B. Zou, *Appl. Catal. B* **2013**, *134*, 293–301.
[33] L. Zhao, T. Cui, Y. Li, B. Wang, J. Han, L. Hanb, Z. Liu, *RSC Adv.* **2015**, *5*, 64495–64502.
[34] R. Michal, E. Dworniczek, M. Caplovicova, O. Monfort, P. Lianos, L. Caplovic, G. Plesch, Appl. Surface Sci. **2016**, *371*, 538–546.
[35] Z. Yan, Z. Xu, B. Cheng, C. Jiang, *Appl. Surface Sci.* **2017**, 404, 426–434.
[36] K. W. Goyne, A. R. Zimmerman, B. L. Newalkar, S. Komarneni, S. L. Brantley, J. Chorover, *J. Porous Mater.* **2002**, *9*, 243–256.
[37] L. Zhang, Z. Gao, C. Liu, Y. Zhang, X. Z. Tu, X. Yang, F. Yang, Z. Wen, L. Zhu, R. Liu, Y. Li, L. Cui, *J. Mater. Chem. A* **2015**, *3*, 2794–2801.
[38] J. Deng, L. Wang, Z. Lou, T. Zhang, *J. Mater. Chem. A* **2014**, *2*, 9030–9034.
[39] H. Praliaud, S. Mikhailenko, Z. Chajar, M. Primet, *Appl. Catal.* B **1998**, *16*, 359–374.
[40] H. Irie, S. Miura, K. Kamiya, K. Hashimoto, *Chem. Phys. Lett.* **2008**, *457*, 202–205.
[41] C. Huang, L. Chen, K. Cheng, G. Pan, *J. Mol. Catal. A: Chem.* **2007**, *261*, 218–224.
[42] B. Bharti, S. Kumar, H.-N. Lee, R. Kumar, Sci. Report **2016**, *6:32355*, 1–12.
[43] J. Cao, B. Xu, H. Lin, B. Luo, S. Chen, *Dalton Trans.* **2012**, 41, 11482–11490.
[44] M. Lu, C. Shao, K. Wang, N. Lu, X. Zhang, P. Zhang, M. Zhang, X. Li, Y. Liu, *ACS Appl. Mater. Interfaces* **2014**, *6*, 9004–9012.
[45] A. Kumar, T. Mohanty, *J. Phys. Chem. C* **2014**, *118*, 7130–7138.
[46] R. Sahay, J. Sundaramurthy, P. S. Kumar, V. Thavasi, S. G. Mhaisalkar, S. Ramakrishna, *J. Solid State Chem.* **2012**,*186*, 261–267.
[47] N. A. M. Barakat, M. S. Khil, F. A. Sheikh, H. Y. Kim, *J. Phys. Chem. C* **2008**, *112*, 12225–12233.

[48] J. Zhou, F. Ren, S. Zhang, W. Wu, X. Xiao, Y. Liua, C. Jiang, *J. Mater. Chem. A* **2013**, *1*, 13128–13138.
[49] J. Wang, W. Zhu, Y. Zhang, S. Liu, *J. Phys. Chem. C* **2007**, *111*, 1010–1014.
[50] B. Naik, K. M. Parida, C. S. Gopinath, *J. Phys. Chem. C* **2010**, *114*, 19473–19482.
[51] S. Livraghi, M. C. Paganini, E. E. Giamello, A. A. Selloni, C. D. Valentin, G. J. Pacchioni, J. *Am. Chem. Soc.* **2006**, *128*, 15666–15671.
[52] C. S. Gopinath, *J. Phys. Chem. B* **2006**, *110*, 7079–7080.
[53] M. Sathish, B. Viswanathan, R. P. Viswanath, C. S. Gopinath, *Chem. Mater.* **2005**, *17*, 6349–6353.
[54] J. A. Rodriguez, T. Jirsak, J. Dvorak, S. Sambasivan, D. J. Fischer, *Phys. Chem. B* **2000**, *104*, 319–328.
[55] B. Naik, K. M. Parida, *Ind. Eng. Chem. Res.* **2010**, *49*, 8339–8346.
[56] Y. Li, Z. Wanga, X.–J. Lv, *J. Mater. Chem. A* **2014**, *2*, 15473–15479.
[57] H. Hou, M. Shang, F. Gao, L. Wang, Q. Liu, J. Zheng, Z. Z. Yang, W. Yang, *ACS Appl. Mater. Interfaces* ***2016***, *8*, 20128 – 20137.
[58] G. Li, N. M. Dimitrijevic, L. Chen, T. Rajh, K. A. Gray, *J. Phys. Chem. C* **2008**, *112*, 19040–19044.
[59] T. Warang, N. Patel, A. Santini, N. Bazzanella, A. Kale, A. Miotello, *Appl. Catal. A: General* **2012**, *423–424*, 21–27.
[60] B. Huang, W. Yang, Y. Wen, B. B. Shan, R. Chen, *ACS Appl. Mater. Interfaces* **2015**, *7*, 422–431.
[61] G. Yang, Z. Jiang, H. Shi, T. Xiao, Z. Yan, *J. Mater. Chem.* **2010**, *20*, 5301–5309.
[62] X. -Z. Bu, G.-K. Zhang, Y. -Y. Gao, Y. -Q. Yang, *Micropor. Mesopor. Matter* **2010**, *136*, 132–137.
[63] V. Usha, S. Kalyanaraman, R. Thangavel, R. Vettumperumal, *Superlattices and Microstruct.* **2015**, *86*, 203–210.
[64] Y. Liu, G. Zhu, B. Ge, H. Zhou, A. Yuan, X. Shen, *CrystEngComm* **2012**, *14*, 6264–6270.
[65] W. Dong, S. -P. Yen, J. -A. Paik, J. Sakamoto, *J. Am. Ceram. Soc.* **2009**, *92*, 1011–1016.
[66] W. S. Rader, L. Soiujic, E. B. Miiosavijevlc, J. L. Hendrlx, *Environ. Sci. Technol.* **1993**, *27*, 1875–1879.
[67] Y. Xu, M. Schoonen, *Am Mineral* **2000**, *85*, 543–556.
[68] X. H. Li, M. Antonietti, *Chem. Soc. Rev.* **2013**, *42*, 6593–6604.
[69] H. Katsumata, Y. Oda, S. Kanecoa, T. Suzuki, *RSC Adv.* **2013**, *3*, 5028–5035.
[70] K. Liu, C. -Y. Su, T. -P. Perng, *RSC Adv.* **2015**, *5*, 88367–88374.
[71] S. P. Lim, A. Pandikumar, N. M. Huang, H. N. H. Ngee Lim, G. Gud, T. L. Mad, *RSC Adv.* **2014**, *4*, 48236–48244.
[72] Z. Jinfeng, Y. Yunguang, L. Wei, *Int. J. Photoenergy* **2012**, 2012, 1–9.
[73] S. P. Lim, A. Pandikumar, H. N. Lim, R. Ramaraj, N. M. Huang, *Sci. Report* **2015**, *5:11922*, 1 – 14.
[74] X. Qiu, M. Miyauchi, K. Sunada, M. Minoshima, M. Liu, Y. Lu, D. Li, Y. Shimodaira, Y. Hosogi, Y. Kuroda, K. Hashimoto, *ACS Nano* **2011**, *6*, 1609–1618.
[75] Y.–Y. Lau, Y.–S. Wong, T.–T. Teng, N. M. Morad, S.–A. O. Rafatullah, *RSC Adv.* **2015**, *5*, 34206–34215.
[76] T. Shen, C. Jiang, C. Wang, J. Sun, X. X. Wang, X. A. Li, *RSC Adv.* **2015**, *5*, 58704–58712.
[77] D. Tahir, Sven Tougaard, *J. Phys.: Condens. Matter.* **2012**, *24*,1–8.

Submitted: July 26, 2017
Revised: August 4, 2017
Accepted: August 8, 2017